京都大学防災研究所年報 第 50 号 B 平成 19 年 4 月
Annuals of Disas. Prev. Res. Inst., Kyoto Univ., No. 50 B, 2007

Tide-Surge-Wave Coupling Model and Its Application to Surge and Wave Hindcast for Typhoon 0603

Sooyoul KIM, Tomotsuka TAKAYAMA, Tomohiro YASUDA and Hajime MASE

Synopsis

Tide-surge-wave coupling model has been developed to predict surges, tides and waves due to typhoons, which is composed of a depth integrated two dimensional surges/tides model and a wave model (SWAN). A wave dependent drag coefficient and a radiation stress are included in momentum equations, while wave parameters are predicted by currents and water levels. For the purpose of the high resolution the nested scheme from the ocean to the coast is employed to the coupling model by Massage Passing Interface (MPI). A typhoon model and a tidal model provide winds and atmospheric pressures, and tides, respectively. The coupling model is validated by hindcasting Typhoon 0603 which hit the southwest of Korea in 2006. The result of hindcast simulation shows a good agreement with the observation. We expect that the coupling will serve as a risk assessment for coastal disasters due to extreme typhoons.

Keywords: storm surge, wave, tide, coupling model, wave dependent drag coefficient, radiation stress, nesting scheme, MPI, parallel computing

1. Introduction

Since the numerical modeling of the storm surge is developed and applied to the coastal area from the ocean, the effort of many researches has been concerned with the accurate hindcast and forecast of storm surges and waves. Flather (1994) showed that the timing of cyclone landfall and its coincidence with high tide determine the area worst affected by flooding. In addition, he introduced that the differences in tracks and tidal conditions are to be important in a large area of the southern delta in 1970 and along the mainland coast south of Chittagong in 1990 by the comparison with two cyclones. On the other hand, Mastenbroek et al. (1993) studied the effect of a wave dependent drag coefficient on the generation of storm surges in the North Sea using the wave (WAM) and depth averaged Reynolds equation model. They clearly showed that the calculation with the wave dependent drag gives a significant improvement and preferred to a wave dependent drag for a storm surge modeling. Zhang et al. (1996) studied the interaction of waves and currents by the dynamical coupling of a third generation wave model and a two dimensional storm surge model. They also showed that the wave dependent drag coefficient improves the accuracy of computed results. Choi et al. (2003) has established a coupled wave, tide and surge model composed of the two dimensional tide and surge model and wave model (WAM-Cycle 4) in order to investigate the effect of tides, storm surges and wind waves interactions during a winter monsoon in 1983 using the effective drag coefficient of the bottom stress.

In the study, we have developed a tide-surge-wave coupling model composed of: depth integrated two dimensional nonlinearly shallow water equation model; Simulating Wave Nearshore model (SWAN). For the purpose of high resolution, the nested scheme is employed by Massage Passing Interface (MPI) in order to predict waves, tides and surges from the ocean to the coast. Hence, the main coupling model is composed of

several sub-coupling models that have the identical number to the number of computational domains. At section 2, the coupling model will be described. At section 3 and 4 the coupling model is applied to Korea and validated by hindcasting Typhoon 0603 which hit the southwest of Korea in 2006.

2. Tide-Surge-Wave coupling model

Following models are incorporated to a sub-coupling model to calculate surges, tides and waves. In order to reflect the complex topography and obstacles the nested scheme is employed to the coupling model. Each sub-coupling model is simultaneously parallelized by MPI to reduce the labour effort and time. In the study, four computational domains were used and hence, four sub-coupling models were parallelized.

2.1. Hydrodynamic model

The hydrodynamic model developed by Goto et al. (1993) is modified to predict storm surges and tides. It is a two dimensional, depth integrated nonlinear shallow water equations model.

$$\frac{\partial \eta}{\partial t} + \frac{\partial M}{\partial x} + \frac{\partial N}{\partial y} = 0 \tag{1}$$

$$\frac{\partial M}{\partial t} + \frac{\partial}{\partial x}\left(\frac{M^2}{d}\right) + \frac{\partial}{\partial y}\left(\frac{MN}{d}\right) + gd\frac{\partial \eta}{\partial x} = fN - \frac{1}{\rho} d\frac{\partial P}{\partial x} + \frac{1}{\rho}(\tau_s^x - \tau_b^x + F_x) + A_h\left(\frac{\partial^2 M}{\partial x^2} + \frac{\partial^2 M}{\partial y^2}\right) \tag{2}$$

$$\frac{\partial N}{\partial t} + \frac{\partial}{\partial x}\left(\frac{NM}{d}\right) + \frac{\partial}{\partial y}\left(\frac{N^2}{d}\right) + gd\frac{\partial \eta}{\partial y} = -fM - \frac{1}{\rho} d\frac{\partial P}{\partial y} + \frac{1}{\rho}(\tau_s^y - \tau_b^y + F_y) + A_h\left(\frac{\partial^2 N}{\partial x^2} + \frac{\partial^2 N}{\partial y^2}\right) \tag{3}$$

in which η = the sea surface fluctuation, M and N = the depth integrated currents in the x and y direction, P = the atmospheric pressure, f = the Coriolis parameter, g = the gravitational acceleration, $d=\eta+h$ = the total depth, A_h = the horizontal eddy diffusion and ρ = the density of water. F_x and F_y represent the components of the wave induced force which are the functions of the radiation stress in x and y space.

The bottom stresses is represented by

$$\tau_b = \rho_w g n^2 \frac{U|U|}{d^{7/3}} \tag{4}$$

where n is the Manning coefficient, which 0.025, 0.02 and 0.015 were used to computational domains through the trial-error for the high resolution.

The surface stress is usually represented by the following form

$$\tau_s = \rho_a C_D W_{10}|W_{10}| \tag{5}$$

in which W_{10} is the wind speed measured at 10m above the sea surface. In the coupling model, C_D in Eq. (5) is replaced by the wave dependent drag coefficient introduced by Janssen (1989, 1991). The boundary condition is given by zero flow normal to a solid boundary. The somefeld explicit method for the radiation condition is applied to open boundaries (Miller and Thorpe, 1981).

The disturbed water surface at an open boundary is given by

$$\eta_n = \eta_{tide} + \eta_{storm\ surge} = \eta_{tide} + (p_a - p_0)/g\rho \tag{6}$$

where p_a and p_0 represent 1013 hPa and the atmospheric pressure at the open boundary, respectively. H_{tide} is imposed by the ocean tide model for a regional model around Japan developed by Matsumoto (2000) which can make the realistic tide prediction. The wet/dry scheme is also applied for the sake of tidal flat simulation as follows: *if* $(D = h + \eta) \le 0.0005$ $\Rightarrow D = 0$, in which D represents the water depth, h; the mean water level and η; the water surface elevation.

(1) Wind stress

Following the theory of Janssen, the total stress is the sum of a turbulent and a wave-induced stress as follows; $\tau = \tau_{turb} + \tau_w$. Here, τ_{turb} is the turbulent stress, which is modeled by a mixing length hypothesis, $\tau_{turb} = \rho_a (\kappa z)^2 (\partial U / \partial z)^2$, where κ (=0.4) is the von Karman constant and $U(z)$ the wind speed at height z. Based on the numerical results of Janssen, the velocity

profile still has a logarithmic shape for the young wind sea and is deviated from the profile of turbulent air flow over a flat plate. The velocity profile is assumed as follows;

$$U(z)=\frac{u_*}{\kappa}\ln\left(\frac{z+z_e-z_0}{z_e}\right) \tag{7}$$

where $u_* = \sqrt{\tau / \rho_a}$. U_* is the friction velocity and z_0 represents the roughness length. The effective roughness length z_e at $z = z_0$ depends on z_0 and the sea state through the wave induced stress τ_w and the total surface stress τ .

$$z_e = \frac{z_0}{\sqrt{1-\tau_w/\tau}} \tag{8}$$

in which $z_0 = \hat{\alpha}\, u_*^2 / g$ is a Charnock-like relation. $\hat{\alpha}$ is constant and 0.01. Since the drag coefficient defined by

$$C_D = u_*^2 / U(L)^2 = \left[\frac{\kappa}{\ln\frac{z+z_e-z_0}{z_e}}\right]^2 \tag{9}$$

which is fully determined by the roughness length where $U(L)$ is the wind speed given at L and then, the drag coefficient C_D in Eq. (9) is alternatively used on the coupling model instead of that in Eq. (5). The wave stress vector τ_w is determined by

$$\tau_w = \rho_w \int_0^{2\pi}\int_0^{\infty} \omega S_{in}(\sigma,\theta)\frac{\bar{k}}{k}\, d\sigma d\theta \tag{10}$$

where σ is the angular frequency, S_{in} is the wind input source function, and k and $\bar{k}$ represent the wave-number of a wave component and the mean wave-number, respectively. In the SWAN the iterative procedure of Mastenbroek (1993) is used to determine the surface stress, through this iterative procedure from Eqs. (7) to (10).

The radiation stress represents the contribution of the wave motion to the mean flux of horizontal momentum. It is represented by the wave spectrum as follows;

$$S_{xx} = \rho g \int\int \left[\frac{C_g}{C}\cos^2\theta + \frac{C_g}{C} - \frac{1}{2}\right] E\, d\sigma d\theta \tag{11}$$

$$S_{xy} = S_{yx} = \rho g \int\int \left[\cos\theta \sin\theta\right] E\, d\sigma d\theta \tag{12}$$

$$S_{yx} = \rho g \int\int \left[\frac{C_g}{C}\cos^2\theta + \frac{C_g}{C} - \frac{1}{2}\right] E\, d\sigma d\theta \tag{13}$$

in which C represents the wave celerity and C_g the wave group velocity. Therefore, the wave induced forces due to radiation stress on the momentum equations (2) and (3) are as follows

$$F_x = -\frac{\partial S_{xx}}{\partial x} - \frac{\partial S_{xy}}{\partial y} \tag{14}$$

$$F_y = -\frac{\partial S_{yx}}{\partial x} - \frac{\partial S_{yy}}{\partial y} \tag{15}$$

2.2. Typhoon model

Takayama (2002) explained typhoon models of Fujita, Myers and Mitsuda-Fujii in detail. He described that the difference of the wind distribution calculated from three models is very small under the same condition, resulting in the similar wind distribution and wind speed. From this reason, Fujita model is employed to produce the atmospheric pressure and the wind distribution of the typhoon in this study.

The pressure field from the center of typhoon is determined by

$$p = p_\infty - \frac{\Delta p}{\sqrt{1+(r/r_0)^2}} \tag{16}$$

where p_∞ and Δp represent the environmental pressure far from its center and the pressure gradient in space, and r and r_0 denote the radial distance at a station and the radius of the maximum wind speed from the typhoon center, respectively. The gradient of wind is calculated by

$$V_{gr} = r\left[\sqrt{\frac{f^2}{4}+\frac{\Delta p}{\rho_a r_0^2}\left\{1+\left(\frac{r}{r_0}\right)^2\right\}^{-3/2}} - \frac{f}{2}\right]. \tag{17}$$

Finally, the wind speeds at 10m above the sea surface is represented by the vector summation between the gradient wind speed reduced by the sea or land surface friction and the wind speed affected by the moving speed of typhoon. Those are determined by

$$W_x = C_1 V \exp\left(-\frac{\pi r}{l}\right)\cos\theta_t - C_2 V_{gr}\frac{X+\sqrt{3}Y}{2r} \quad (18)$$

$$W_y = C_1 V \exp\left(-\frac{\pi r}{l}\right)\sin\theta_t + C_2 V_{gr}\frac{\sqrt{3}X-Y}{2r} \quad (19)$$

2.3. Wave model

A third-generation numerical wave model (SWAN) to compute random, short-crested waves in coastal regions with shallow water and ambient current was developed and verified by Booij et al. (1999). The model can be applied to coastal regions with shallow water, islands, tidal flats and local wind as well as with horizontal scales less than 20-30km and water depths less than 20-30m. In addition, SWAN can be used on any scale relevant for wind generated surface gravity waves.

This model accounts for shoaling, refraction, generation by wind, whitecapping, triad and quadruplet wave-wave interactions, and bottom and depth-induced wave breaking. The basic equation in SWAN is the wave action balance equation and is given by

$$\frac{\partial}{\partial t}N+\frac{\partial}{\partial x}c_x N+\frac{\partial}{\partial y}c_y N+\frac{\partial}{\partial \sigma}c_\sigma N+\frac{\partial}{\partial \theta}c_\theta N=\frac{S}{\sigma} \quad (20)$$

in the Cartesian coordinates (x, y). Here, N (σ ,θ) is the action density spectrum, c_x and c_y present the group velocities in x and y direction, C_σ and C_θ also present the one in σ and θ direction and S is the source terms. T is the time, x and y present the space in geographic grid, in contrast with σ and θ are the frequency and its direction of a wave component.

Time is discretized with a simple constant time step for the simultaneous integration of the propagation and the source terms in contrast with it in the WAM model or the WAVEWATCH model. The discrete frequencies are defined between a fixed low-frequency cutoff (typically, f_{min}=0.04Hz) and a fixed high-frequency cutoff (typically, f_{max}=1.0Hz) which are defined by the user and computed by SWAN, respectively. SWAN allows the use of nested grids to provide high-resolution results at desired locations and provides estimates of wave setup due to radiation stress.

Lalbeharry et al. (2004) showed that the modified version of the SWAN implementation of WAM4 produces wave heights that are more accurate than those of the unmodified version by applying the wave growth limiter in the exponential wind growth source term on WAM 4.5 to one instead of the original limiter described by Ris (1997) on SWAN. The shift growth parameter Z_α=0.0011 is also included. The original limiter implemented on SWAN and the limiter on WAM4.5 are

$$\left|\Delta N(\sigma,\theta)\right|_{\max} = (0.1\alpha_{PM})/(2\sigma k^3 c_g) \quad (21)$$

$$\left|\Delta N(\sigma,\theta)\right|_{\max} = (2\pi)^2 \times 3.0\times10^{-7} g u_* \sigma_c \Delta t/(\sigma^3 k) \quad (22)$$

Instead of Eq.(21), Lalbeharry et al. applied Eq.(22) to SWAN. In the study, the modified limiter and the shift growth parameter is employed to improve the accuracy of the significant wave heights.

2.4 Grid refinement

Open boundary values on the fine domain are linearly interpolated from the coarse domain (Kowalik et al., 1993). The nesting of the different domains is non-interactive (passive) and the variables calculated in the coarser-grid domain are passed to the finer resolution domain only.

2.5. Coupling process

A main coupling model is composed of the same number of sub-coupling models with the number of domains used in the computation. For example, if the four computational domains from the ocean to coast region are used for the hindcast simulation, the framework of the main coupling model is constructed by four sub-coupling models. Each sub-model is successively run by paralleling them using MPI.

During the coupling process the wave dependent drag and the radiation stress are transferred to the corresponding position on the grid of the storm surge model. The water level and currents are additionally transferred to the matching position on the grid of SWAN. Typhoon model provides the wind and the atmospheric pressure distribution to the coupling model.

The computation process of a main model composed of k_i sub-coupling models, which i = 1, N, is as follows (Fig. 1):

(1) Storm surge/tide model preliminary computes only tides from domain 1 to N.

(2) The wave model in the k_1 sub-coupling model runs under currents and water level of the same sub-coupling model to obtain waves. The wave model in the k_2 sub-coupling model conducts the computation with open boundary values obtained from the k_1 sub-coupling model and currents and water level of the k_2 sub-coupling model. The process repeats by the K_N sub-coupling model.

(3) New wave dependent drag and radiation stress of each wave model in each K_i sub-model are given to each corresponding storm surge model at the next time step.

(4) The storm surge model in the k_1 sub-coupling model is run by the wave dependent drag and the radiation stress of the k_1 sub-coupling model. The storm surge model in the k_2 sub-coupling model carries out the computation using the water level imposed on open boundaries by the k_1 sub-coupling model, and the wave dependent drag and radiation stress of the k_2 sub-model. The process repeats from the k_1 to k_N sub-coupling model.

(5) New currents and water surface elevation obtained from each storm surge model in each k_i sub-coupling model are transferred to each corresponding wave model at the next time step.

(6) The processes from (2) to (5) are repeated during the computation.

3. Application to Korea

3.1 Hindcast simulation of Typhoon 0603 (Ewiniar)

The hindcast of Typhoon 0603 (Ewiniar) was conducted to confirm the applicability of the coupling model. Typhoon 0603 (Ewiniar), which hit the western coastal sea of Korea in 2006, was selected to validate the hindcast simulation in comparison with the observation. As listed in Table 1, Typhoon 0603 (Ewiniar) was born on UTC 30 June in 2006 near 7.5° N 137.8° E The tropical storm born at UTC 1 July changed to the typhoon near 14° N 136° E at UTC 3 July. The typhoon moved northwestward, turned northeastward at UTC 9 July and hit the southwest of Korea on UTC 10 July in 2006 with the central atmospheric pressure of 975hPa. The typhoon passed through the middle of the western coastal region and disappeared on the East Sea (Japan Sea) on 11 July. The wind speed of 25m/s was recorded at the western coastal sea of Korea. The typhoon remained the life loss and missing of 8 persons, and caused the inundation and the property damage of 600,000 USD in Korea. Figure 2 shows the track of Typhoon 0603 (Ewiniar). The storm surge simulation for the hindcast of Typhoon 0603 (Ewiniar) is conducted from 18:00 06 July to UTC 06:00 11 July 2006. In order to reproduce the wind and atmospheric field of Typhoon 0603 (Ewiniar), the atmospheric pressure data observed on the sea surface by Japan Meteorological Agency and Korea Meteorological Administration are used. Figure 3 shows the observation points of the wave and tide around Korean peninsula.

Table 2 shows the status of observation stations. Three stations were chosen for waves and five stations were done for the storm surge. The station (3) for the wave and (e) for the tide were located on 4th domain,

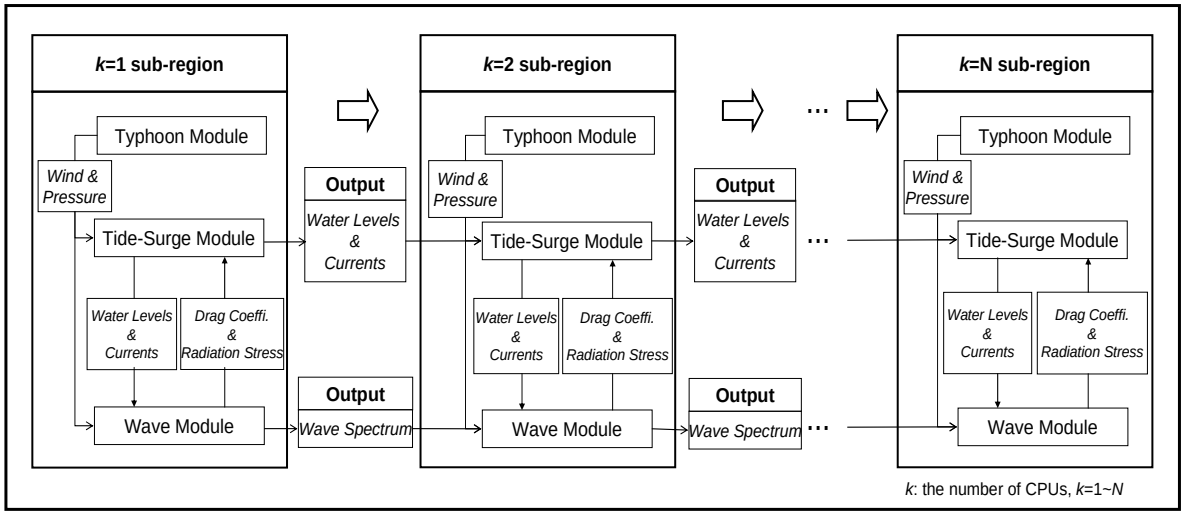

Fig. 1 The framework of the main coupling model.

while the other stations were located in first domain. The resolutions of about 300m to 10km were employed to produce the wave and the storm surge (see Table 3). Ministry of Maritime Affairs Fisheries (MMAF) in Korea provides the observation data on the internet and is available to access at any time. The computational domain is shown in Fig. 4 and four domains are used to predict waves, tides and surge due to Typhoon 0603.

Table 1 Track of Typhoon 0603.

TIME(UTC)	Latitude (˚N)	Longitude (˚E)	Pressure (hPa)
2006070700	208	1276	950
2006070706	214	1274	950
2006070712	221	1271	950
2006070718	225	1265	950
2006070800	231	1266	950
2006070806	241	1263	950
2006070812	251	1261	955
2006070818	263	1259	955
2006070900	275	1258	960
2006070906	293	1258	960
2006070912	306	1258	965
2006070918	316	1257	965
2006071000	336	1261	975
2006071006	355	1265	985
2006071012	368	1270	990
2006071018	382	1283	994
2006071100	402	1314	996

Table 2 The status of the stations (W: wave, T: tide).

No.	Station	Latitude (N)	Longitude(E)
(1)	Iedo (W)	32-07-23	125-10-57
(2)	Pusan (W)	35-07-47	129-08-16
(3)	Sucheon (W)	36-07-12	126-32-24
(a)	Seoguipo (T)	33-14-12	126-33-49
(b)	Jeju (T)	33-31-27	126-32-43
(c)	Pusan (T)	35-05-35	129-02-15
(d)	Sokcho (T)	38-12-16	128-35-48
(e)	Gunsan (T)	35-58-06	126-37-36

Table 3 Computational domains

Domain	Grid size	Num. grids
1	Δx = 11,100m Δy = 11,100m	151×211
2	Δx = 3,700m Δy = 3,700m	52×42
3	Δx = 1,233m Δy = 1,233m	88×64
4	Δx = 411.1m Δy = 411.1m	115×101

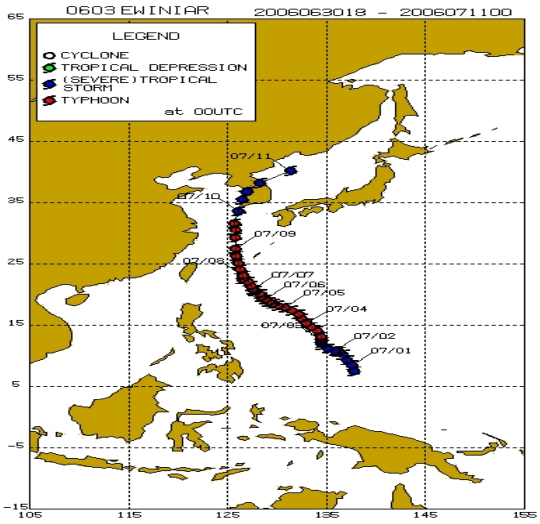

Fig. 2 The track of Typhoon 0603 (UTC).

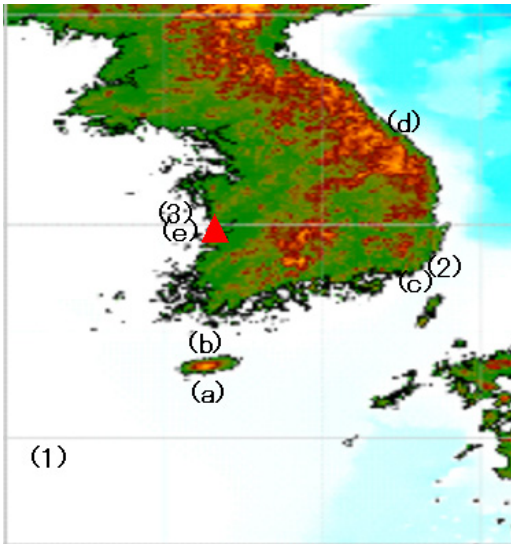

Fig. 3 The observation stations around Korea Peninsula (wave; (1), (2) and (3), tide; (a), (b), (c), (d) and (e)).

4. Result of hindcast simulation

The storm surge, wave and tide generated by Tyhpoon 0603 (Ewiniar) were hindcasted for 5 days starting from UTC 18:00 on 06 July by the coupling model. Before the coupling procedure started, the tide was first calculated to distribute the steady state through all domains.

Once the tide was sufficiently steady, the coupling model begun to calculate the storm surge and wave propagation with the tide imposed on open boundary. For tide/surge model 10 seconds are used, whereas for SWAN 300 seconds are employed. The transfer time between two models was used as 300 seconds. A resolution of 10° was used in the directional space on

SWAN.

As listed on Table 2, the results of coupling model at stations (1), (2), (a), (b), (c) and (d) were obtained on the first domain. On the other hand, the results at stations (3) and (e) were achieved on the fourth domain. The observation data such as the wind, atmospheric pressure, significant wave height and storm surge are obtained from National Oceanographic Research Institute (NORI) in Korea.

4.1. Meteorological data

The results from the hindcast simulation of Typhoon 0603 (Ewiniar) on the first and fourth domain were compared with the observation and these provided the information of the storm surge at the coastal region where the typhoon passed through. Before the results were discussed, the meteorological data were described with the comparison with the observation.

Figure 5 shows the meteorological data observed at Iedo of (1) as shown in Fig. 3. The maximum depression of the atmospheric pressure at the center of Typhoon 0603 (Ewiniar) was about 968 hPa. On the other hand, the storm surge simulation produced that of 978 hPa.. In addition to the magnitude of the atmospheric pressure, the maximum depression of the simulation generated later about 3hours. From this fact, the difference of the storm surge between the hindcast prediction and the observation might occur more than 0.1m near Iedo, because it is assumed that 1 hPa = 1cm. Unfortunately, the observation of the wind velocity could not be done until 12:00 10 July in 2006, but started after that. Unlike the wind speed, the wind direction had been observed during the storm event. The direction of wind was relatively good agreement with the observation when the typhoon passed through

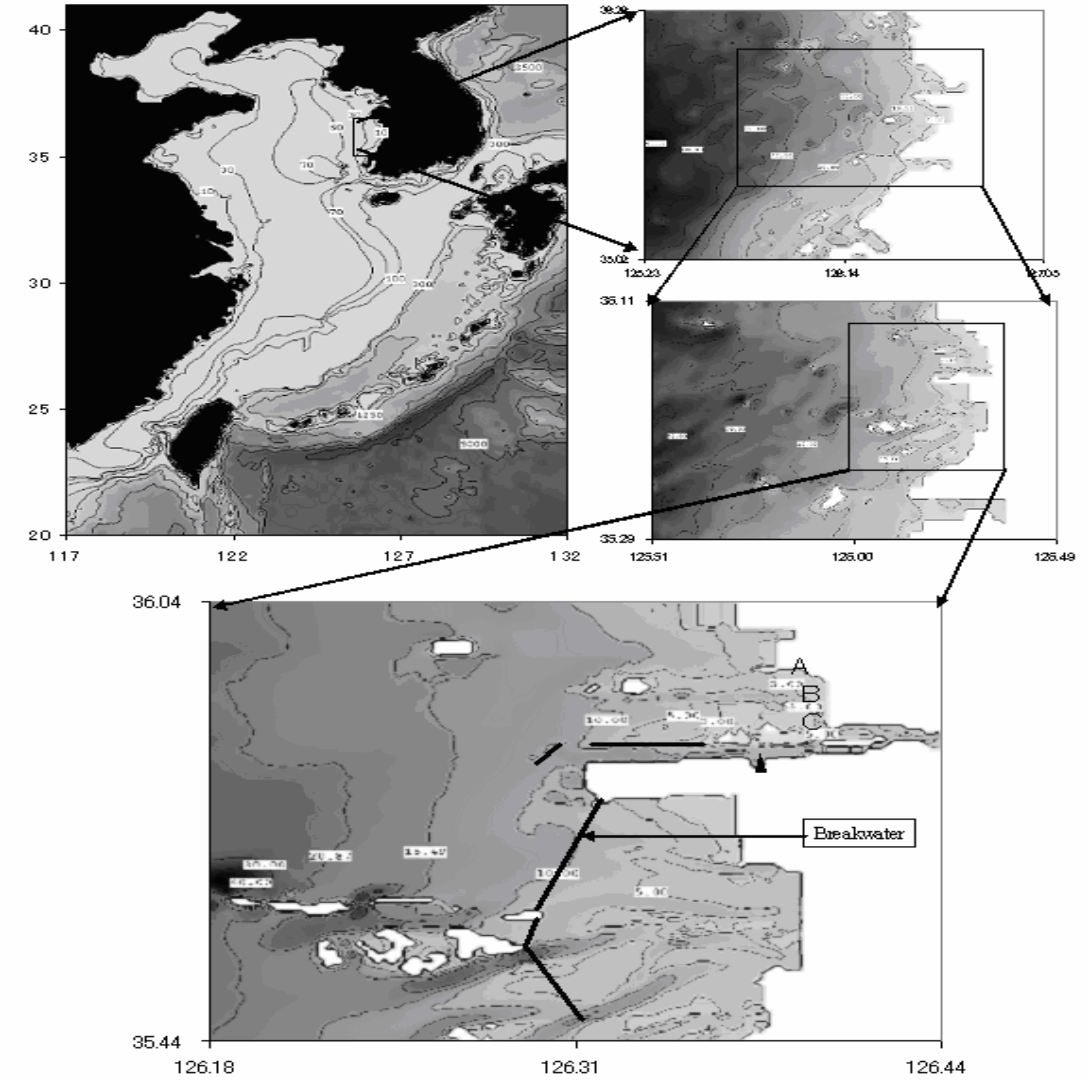

Fig. 4 Four levels of geographic regions.

Iedo. The observed wind direction was rapidly changed in comparison with the prediction before and after at 2:00 7 July.

Figure 6 shows the meteorological data observed at Pusan of (2) in the first domain. It was estimated that the pressure of 996 hPa fairly produced by the simulation in comparison with the observed atmospheric pressure of 993 hPa at 13:00 7 July. Although the observed wind speed showed the local change in its direction, the overall predicted wind speed was well produced by the simulation. Especially, the maximum wind speed of 18m/s in the simulation was good agreement with the observation. Until 0:00 10 July, the rapid change of the wind direction occurred. When the typhoon passed through around Pusan located on the right side of its track, the wind direction changed to blow from the east toward the west.

The predicted meteorological data at Sucheon had the highest resolution of about 300m in the grid size as shown in Fig. 7. The time lag of the generation in the maximum depression of the pressure was about 6 hours. Typhoon model produced the overestimated maximum depression of the pressure. In addition to the pressure, the predicted wind speed was underestimated before 14:00 10 July and overestimated after that compared to the observation. The overall change of the wind direction in the computation relatively agreed with the observation before 18:00 10 July, but was in disagreement with the observation after that. The observed direction was changed from 270° to 90°, but the computed direction of 270° was not changed after 18:00 10 July.

Until now on, the meteorological data in the computation was compared with the observation at three stations of Iedo, Sucheon and Pusan. At the early stage of the hindcast simulation when the typhoon was on deep sea, the discrepancy between the observation and the computation highly occurred.

4.2. Significant wave height

The significant wave height computed by the coupling model was compared with the observation data. In the study, three observed data were obtained from NORI in Korea. Figure 8 shows that the significant wave height was observed at Iedo of (1) as shown in Fig. 3.

The significant wave height of 6m in the computation showed the good agreement with the observation, until it developed to its peak. After its peak, the observation was rapidly decreased.

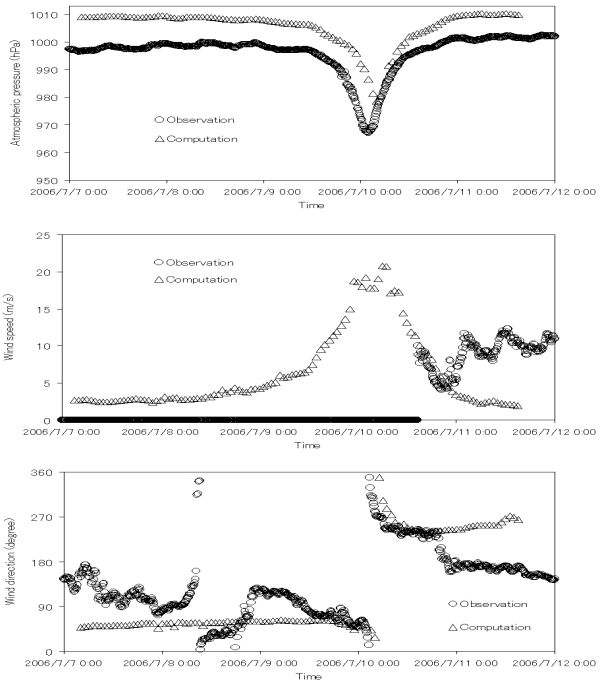

Fig. 5 The meteorological data observed at Iedo of (1) (Upper; the atmospheric pressure, middle; the wind speed, lower; the wind direction).

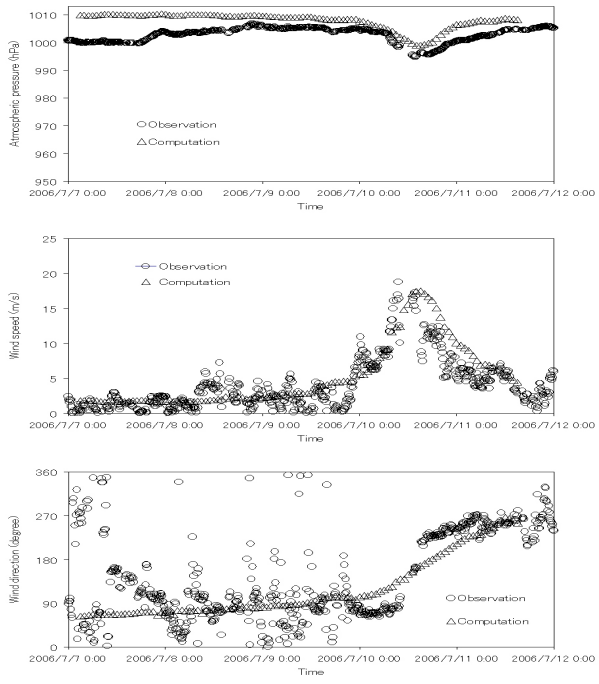

Fig. 6 The meteorological data observed at Pusan of (2) ((Upper; the atmospheric pressure, middle; the wind speed, lower; the wind direction).

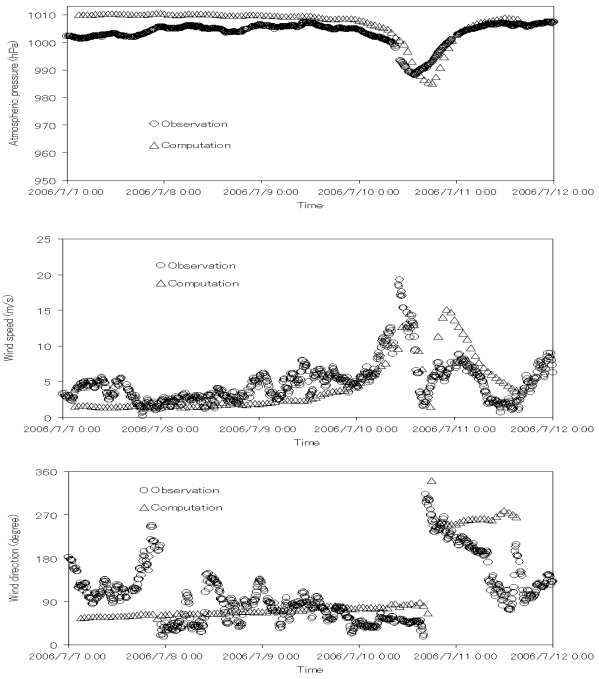

Fig. 7 The meteorological data observed at Sucheon of (3) (Upper; the atmospheric pressure, middle; the wind speed, lower; the wind direction).

Although those peaks of the observation and the computation significantly agreed, they showed the discrepancy after 0:00 10 July. Based on the wind speed and direction in Fig. 6, it was expected that the observed wind speed and direction should resulted in those discrepancy between the result of the computation and the observation, even though the wind speed was not observed actually.

Although the predicted meteorological data showed the good agreement with the observation at Pusan of Fig 9, the peak of the observed significant wave height was 7m high. On the other hand, the predicted peak was 4m. The discrepancy between both was quite large. It was estimated that the computation of wave could not produce the shoaling, because of the resolution of 10km in the computational domain 1. Therefore, waves in the computation could not propagate sufficiently from the deep to coastal sea, even though the wind speed and direction computed by the coupling model was well produced at Pusan.

The significant wave height was observed less than 0.7m at Sucheon as shown in Fig. 10. Although the observed wind speed of about 20m/s was not small at Sucheon compared to at Pusan and Iedo, the wind direction, blowing from the land toward the sea, resulted in the small significant wave height developed by the wind. On the other hand, the significant wave height was predicted about 1.0m and overestimated in comparison with the observation after 0:00 11 July.

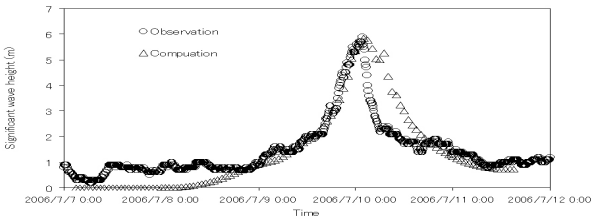

Fig. 8 The significant wave height of the observation and computation at Iedo of (1).

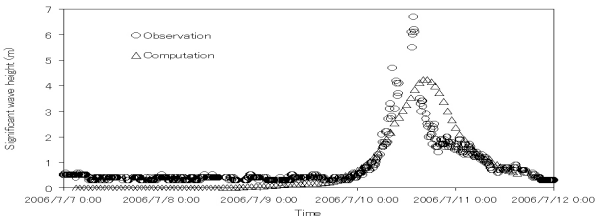

Fig.9 The significant wave height of the observation and computation at Pusan of (2).

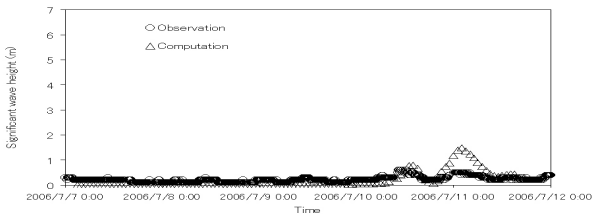

Fig. 10 The significant wave height of the observation and computation at Sucheon of (3).

4.3. Storm surge

At previous sections 4.1 and 4.2, it was discussed that the result of computation in the meteorological data and the significant wave height in the comparison with the observation. Although the prediction at Pusan agreed well with the observation for the meteorological data, the hindcast simulation could not produced sufficiently the significant wave height compared to the observation. The peak of the significant wave height in the computation agreed well with the observation at Iedo where the wind speed could not be observed. In addition, the result did not agree with the observation for the peak of significant wave height and meteorological data at Sucheon where the center of Typhoon 0603 (Ewiniar) passed through.

Jeju and Seoguipo of (b) and (a) as shown in Fig. 3 are located in the Jeju island. Seoguipo is located in the

south coast of Jeju island, while Jeju is in the north coast of Jeju island. Seoguipo and Jeju are first the observation points faced to the effect of the typhoon moving to the Korean Peninsula except Iedo of (1). At the early stage of the generation in the storm surge due to Typhoon 0603 (Ewiniar), the water level started to be disturbed at Seoguipo facing to the open sea. It was also expected that the wind blew from the land as the typhoon approaches. When the typhoon arrived at Jeju island, the maximum storm surge should occur at Seoguipo and Jeju at the same time as shown in Fig. 11 and 12, even though computed tides were larger than the observation. The maximum storm surge generated at both was similar as approximately 0.5m as shown in Fig. 16.

It was expected that the storm surge generated at Gunsan of (c) in Fig. 3 was overestimated by the hindcast simulation in comparison with the meteorological data observed at Sucheon as shown in Fig. 7. Sucheon of (3) is very close to Gunsan of (c) as shown in Fig. 3. The storm surge started to apparently generate after 12:00 10 July and its peak occurred around 22:00 10 July as shown in Fig. 13. The atmospheric pressure and the wind speed were overestimated and then, the wind blew from the sea to the land by the computation. Therefore, the impractical storm surge was predicted by the combination of three factors such as the atmospheric pressure, the wind speed and direction.

In the case of Pusan located in the right side of its track, the water level computed by the simulation agreed well with the observation, even though the significant wave height of the computation was underestimated as 50% of the observation. Although the computed meteorological data agreed well with the observation, the hindcast simulation computed the reasonable water level at Pusan as shown in Fig. 14.

In the case of Sokcho of (d) in Fig. 3, the track of Typhoon 0603 (Ewiniar) passed through Sokcho and the water level increased and oscillated as shown in Fig. 15. The wind should blow from the sea to the land, because the wind around the typhoon blew into its center. However, the water depth in the East Sea (Janpan Sea) is so deep that the magnitude of the storm surge became smaller. Additionally the reason was that the magnitude of the typhoon was weaken when passing through Sokcho.

Figure 16 shows the maximum storm surge occurred at each station. The highest maximum storm surge generated as 0.55m at the station of Seoguipo, while the lowest maximum storm surge of 0.2m occurred at Pusan during the storm event of Typhoon 0603 (Ewiniar).

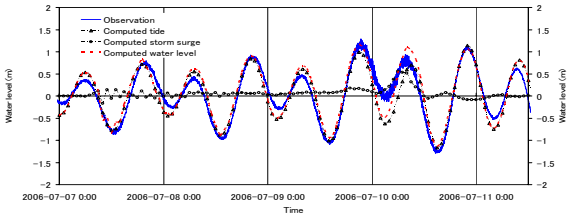

Fig. 11 The water level at Seoguipo of (a).

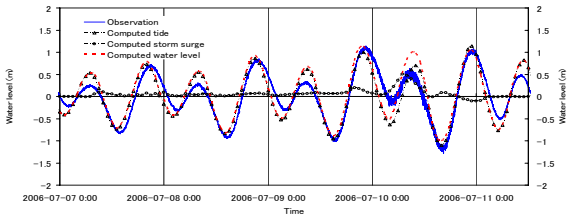

Fig. 12 The water level at Jeju of (b).

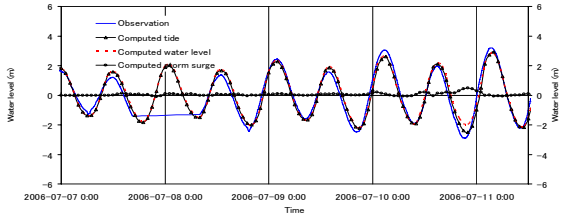

Fig. 13 The water level at Gunsan (e).

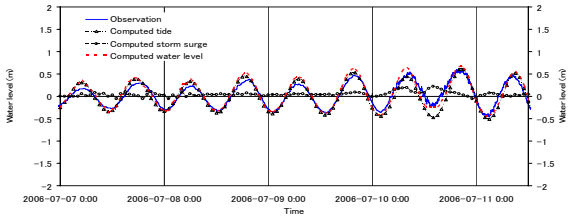

Fig. 14 The water level at Pusan (c).

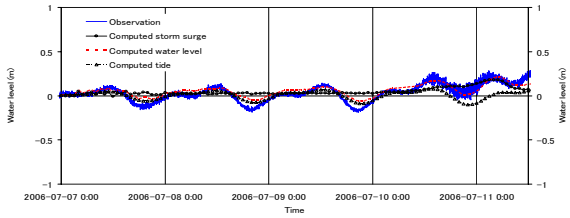

Fig. 15 The water level at Sokcho (d).

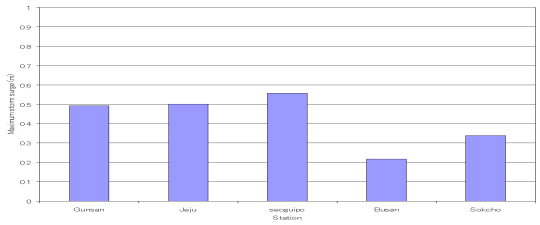

Fig. 16 The maximum storm surge occurred at each station.

5. Summary and conclusions

Tides-waves-surges coupling model has been developed using pre-operational models; two dimensional depth integrated nonlinear shallow water equations model, simulating wave nearshore (SWAN), typhoon model and tidal prediction model. In order to predict surges and tides, a wave dependent drag coefficient and a radiation stress are used. In order to compute significant wave heights, currents and water levels are used. The main coupling model is composed of several sub-coupling models that are simultaneously parallelized by MPI to solve them in the oceanic scale to the coastal scale (the nested scheme).

The coupling model is applied to the Korean peninsula. Storm surges and the waves caused by Typhoon 0603 is hindcasted in order to validate the coupling model. The significant wave height and water level predicted by the coupling model showed relatively the good agreement with the observation.

From the hindcast simulation of Typhoon 0603, we expect that the coupling model will serve as a risk assessment. In the future work it is needed to improve the accuracy of the meteorological data.

6. References

Booij, N., R. C. Ris, and L. H. Holthuijsen (1999). A third-generation wave model for coastal regions. Part 1, Model description and validation, *Journal of Geophysical Res.*, Vol.104, No.C4, pp. 7649-7666.

Choi, B. H., Hyun Min Eum and Seung Buhm Woo: "A synchronously coupled tide-wave-surge model of the Yellow Sea", *Journal of Coastal Engineering*, 47, pp. 381-398, 2003.

Flather, R. A.: "A storm surge prediction model for the Northern Bay of Bengal with application to the cyclone disaster in April 1991", *Journal of physical oceanography*, Vol. 24, pp. 172-190, 1994.

Goto, C., Sato, K. (1993). Development of Tsunami Numerical Simulation System for Sanriku Coast in Japan, *Report of the port and harbor research institute*, Vol.32, No. 2, pp 3-44.

Janssen, P. A. E. M.(1989) Wave-induced stress and the Drag of Air Flow over Sea Waves, *Journal of Physical Oceanography*, 19, pp. 745-754.

Janssen, P. A. E. M. (1991). Quasi-linear Theory of Wind-Wave Generation Applied to Wave Forecasting, *Journal of Physical Oceanography*, 21, pp. 1631-1642.

Kowalik, Z. and Murty, T. S.: Numerical modeling of ocean dynamics, *Advanced series on ocean engineering, vol.5*, 1993.

Lalbeharry, R., Behrens, A., Guenther and H., Wilson, L.: "An evaluation of wave model performances with linear and nonlinear dissipation source terms in lake erie", *Proc. 8th int. workshop on wave hindcasting and forecasting*, Hawaii, USA, 2004.

Mastenbroek, C., G. Burgers, and P. A. E. M. Janssen: "The Dynamical Coupling of a Wave Model and a Storm Surge Model through the Atmospheric Boundary Layer", *Journal of Phys. Oceanogr.*, 23, pp. 1856-1866, 1993.

Matumoto, K., T. Takanezawa and M. Ooe: "Ocean Tide Models Developed by Assimilating TOPEX/POSEIDON Altimeter Data into Hydro-dynamical Model" : A Global Model and A regional Model around Japan, *Journal of Oceanography*, Vol.56, pp 567-581, 2000.

Takayama, T. (2002). Present numerical simulations of storm surge and their problems to solve, *Lecture Notes of the 38th Summer Seminar on Hydraulic Engineering*, 02-B-6, September (in Japaneses).

Zhang, M. Y., and Y. S. Li: "The synchronous coupling of a third-generation wave model and a two-dimensional storm surge model", *Journal of Ocean Eng.*, Vol.23 No.6, pp. 533-543, 1995.

台風0603号による高潮および波浪追算への潮汐・高潮・波浪結合モデルの適用

金　洙列・高山知司・安田誠宏・間瀬　肇

要　旨

高潮予測モデルに，潮汐変動モデルおよび波浪モデルを結合させたモデルを開発した．高潮と潮汐モデルは非線形長波モデルであり，波浪モデルはSWANである．波齢に依存した海面抵抗係数とラディエーションストレスが運動方程式に組み込まれており，海水位や流れと共に計算される．計算の高精度化のために，外洋から沿岸までネスティングスキームを用い，各領域をウィンドウズプラットフォーム上でMPIによって並列計算した．台風モデルによって風および気圧を，潮汐モデルによって潮汐変動をそれぞれ計算する．開発した結合モデルを用いて，2006年に韓国西海岸に来襲した台風0603号（Ewiniar）の追算をし，その適用性を検証した．水位の追算結果は観測値と良い一致を示した．本結合モデルは，極端化台風による沿岸災害についてのリスクアセスメントに用いることができる．

キーワード：潮汐・高潮・波浪結合モデル，海面抵抗係数，ラディエーションストレス，ネスティングスキーム，MPI，並列計算